Environmental Science & Technology

pubs.acs.org/est

Article

Always Lost but Never Forgotten: Gas-Phase Wall Losses Are Important in All Teflon Environmental Chambers

Jordan E. Krechmer,* Douglas A. Day, and Jose L. Jimenez*

Cite This: *Environ. Sci. Technol.* 2020, 54, 12890−12897

Read Online

ACCESS | Metrics & More | Article Recommendations | Supporting Information

ABSTRACT: Yields of secondary organic aerosol (SOA) formation from oxidation of volatile organic compounds are measured in laboratory chambers and then applied in regional and global models. Gas-phase losses to large Teflon-walled environmental chambers have been recently shown to reduce SOA yields. Historically, most chambers have operated in batch mode. Increasingly, however, continuous flow (CF) mode is being used, in which reactants and products are continuously introduced and exhausted from the chamber. Recent literature reports indicate a belief that SOA yields measured in CF chambers are not affected by gas-phase wall losses (GWL). Here, we use an experimentally-constrained box model to show that gas-phase wall losses impact both types of chambers when run under similar conditions. We find CF experiments do mitigate some effects of gas-phase wall losses after long (>2 days) experiment run times, but they have significant losses for typical literature experiment times of 1 day. However, this mitigation phenomenon is an experiment- and mechanism-dependent, and GWL still affects the absolute SOA yield. Finally, we show that at condensation sink values higher than the wall loss rate a lack of change in yield vs seed surface area does not necessarily indicate whether GWL affects the experiment and does not suggest the magnitude.

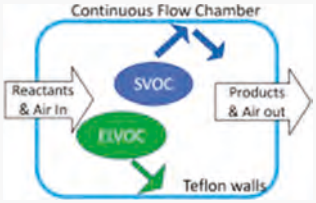

INTRODUCTION

Environmental or "smog" chambers are critical tools for atmospheric chemistry research. The Earth's atmosphere contains tens of thousands of individual organic constituents[1] and air moves and mixes quickly in complex ways, making it too complex to conduct field experiments with sufficient constraints to determine fundamental parameters of interest to atmospheric models. Thus, atmospheric chemists and physicists use reactors such as environmental chambers to isolate one or more chemicals for detailed study.[2] An important application of chambers is the quantification of secondary organic aerosol (SOA) yields from the oxidation of volatile organic compounds (VOCs),[3,4] which are then used in box, regional, and global models.[5,6]

A wide variety of chambers exist with differing shapes, sizes, temperature control systems, and photochemical sources. All chambers operate in one of two flow modes: batch or continuous flow (CF). Chambers that have typically been operated in batch mode include those at Caltech,[7] UC Riverside,[8] the Paul Scherrer Institute,[9] EUPHORE,[10] and the University of Colorado.[11] Batch mode chambers usually have flexible Teflon walls. During experiments, an operator injects reactive chemicals into the chamber at a discrete point in time. The scientist then initiates a reaction or process (e.g., by turning the lights on or by injecting the last reactant needed for the chemistry to start), and instruments draw sample air out of the chamber for measurements. Batch mode chambers are relatively simple to operate, but the length of the experiment and the number of instruments/samplers are limited by the volume of the bag or particle-phase wall losses.

Chambers that always or often operate in continuous flow (CF) mode include SAPHIR,[12] HEC,[13] CLOUD,[14] PNNL,[15] and COALA.[16] CF chambers can operate in "initiation" or "semi-batch" mode, in which a set of precursors and reactants are injected at the beginning of an experiment and the contents are gradually diluted (or reactants continually added), as typically used in the CLOUD and MIT[17] chambers. Or CF chambers can operate in a "steady-state" mode, which is the primary focus of this work and is assumed whenever we discuss "CF" from here on. In CF chambers, new reactants and buffer gases constantly flow into the chamber and the same amount of air is pulled out to sample or discard, maintaining a constant air volume in the chamber. CF chambers can be constructed with rigid walls to enable experiments at different pressures and reducing leaks (e.g., ref 14) and allow for much longer duration experiments than would be possible in batch mode. Although batch mode chambers have been historically more popular and still outnumber CF chambers, over the last decade the use of chambers in CF mode has steadily increased.

Losses of particles to chamber walls have been known for many years, and corrections for these losses are typically applied to chamber yields.[18−20] Until recently, the losses of gas-phase species to the Teflon walls were thought to be of

Received: May 27, 2020
Revised: August 9, 2020
Accepted: September 15, 2020
Published: September 15, 2020

minor importance. Recent works,[21−26] however, have detailed and quantified how gases are lost to the walls of Teflon chambers at relatively fast rates (∼10−15 min time scales). The gas-phase wall loss process can be modeled analogously to equilibrium partitioning,[27] in which the amount of gas that remains in the Teflon walls is determined by the equilibrium vapor pressure of the species in the gas phase at the temperature of the chamber and the type and amount of Teflon chamber wall that is exposed to the gas phase.[21,23]

The recent literature indicates a belief that SOA yields measured in CF chambers are not affected by gas-phase wall losses (GWL) because the walls may potentially reach equilibrium with the semivolatile species, and thus vapor wall losses no longer play a role in the system. This claim is supported by publication of constant yields while varying the aerosol seed surface area for one experimental system.[15]

In this work, we use a box model to investigate the effects of gaseous wall losses on secondary organic aerosol (SOA) chamber yields. We incorporate the latest results in quantifying gas-phase chamber wall losses into the model and constrain a simple SOA base case with a previously published study conducted in a CF chamber.[13] We then run the model in batch and continuous flow versions. We use the results of the model to track the fates of carbon throughout the simulated time periods and determine whether CF chambers suffer from the same wall loss effects as other chambers do. Finally, we perform sensitivity studies to explore the controlling factors for GWL.

EXPERIMENTAL METHODS

Description of the Chamber Box Model. We model a simple, lumped chemical reaction system solved by the KinSim (v. 3.35) chemical kinetic integrator[28] in the Igor Pro 7 environment (Wavemetrics, Lake Oswego, OR, USA). Figure 1 provides an overview of the model with all reactions.

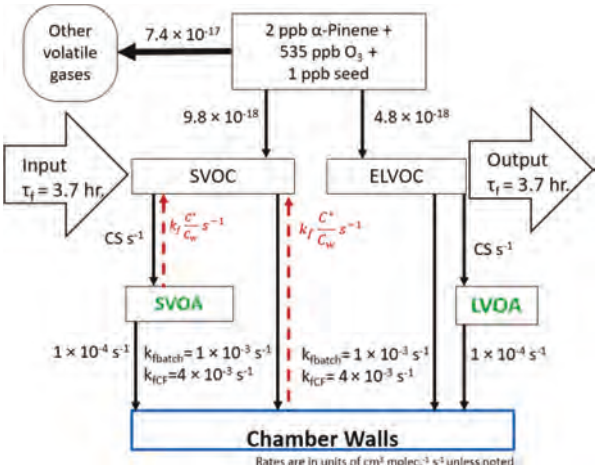

Figure 1. A schematic of the continuous flow model as implemented in this study. The batch model is the same as above, without the input and output flows. The SVOC wall-phase oligomer reaction rate coefficient is set to zero in the base case and turned on in one sensitivity study. Acronyms are as follows: SVOC is semivolatile organic compound, ELVOC is extremely low volatility organic compound, SVOA is semivolatile organic aerosol, and LVOA is low volatility organic aerosol. Partial rate coefficients for α-pinene are in units of cm^3 $molecules^{-1}$ s^{-1}.

The model was inspired by the chamber experiments in Shilling et al.,[13] in which the authors quantified the secondary organic aerosol (SOA) yield from α-pinene oxidation via ozonolysis. As in the original experiments, we simulate a 5 m^3 chamber with a residence time (τ_f) of 3.7 h. The simulations start with 2 ppb of α-pinene and 5 μg m^{-3} of a monodisperse ammonium sulfate seed in the chamber. The model calculates a surface area and condensation sink from the seed aerosol mass, assuming an idealized uniform particle diameter of 85 nm, which was approximately the center point of the SMPS aerosol distribution shown in Figure S1 of Shilling et al.[13] and a molecular weight for ammonium sulfate of 132 g/mol. We then add low volatility organic aerosol (LVOA) and semivolatile organic aerosol (SVOA), calculated using the same size distribution but with molecular weights of 325 and 200 g/mol, respectively. The model does not use the inorganic seed mass to calculate partitioning constants for condensation or evaporation of SVOC or ELVOC species.

Ozone is then introduced at increasing concentrations with the same time dependence as reported in Shilling et al.[13] α-pinene reacts with ozone at a total rate coefficient of 8.8 × 10^{-17} cm^3 $molecules^{-1}$ s^{-1},[29] and we treat the resulting gas-phase products as three lumped species: a semivolatile compound (SVOC; saturation mass concentration C^* = 1 μg m^{-3}); an extremely low volatility compound (ELVOC; very low C^*); and an "other volatile gases" fraction that remains inert and unchanged after the initial reaction. The other volatile gases fraction is supported by other comprehensive measurements[30] and includes volatile gas-phase products that are unlikely to form aerosol at low OA mass concentration levels, such as pinonaldehyde, acetone, acetic acid, formaldehyde, and carbon monoxide. Isaacman-vanWertz et al.[30] also recorded numerous unidentified signals with the PTR-MS, which due to the volatility range of traditional PTR-TOF instruments are likely to be highly volatile and not contribute to aerosol formation.[16]

The SVOC is formed with an 18% mass yield from the reaction of α-pinene and O_3 and the ELVOC with a 9% mass yield. The presence of both SVOC and ELVOC for this system is well supported by the literature.[31,32] The yield values for the base case are in the range of prior studies and were chosen to approximately match the temporal dependence and aerosol production in Shilling et al. (Figure S1).[13] We later perform sensitivity studies vs these yield values.

The rate of vapor loss to the walls is another important parameter. With reasonably high wall accommodation coefficients (α > 6 × 10^{-6}), which are the case for SOA studies,[18] the wall loss rate is the same as the time scale of transport of a molecule to the chamber walls.[23] We use a gas-phase wall loss rate for the SVOC and ELVOC of 1 × 10^{-3} s^{-1} for batch chambers (mixing time scale of ∼1000 s), which is similar to rates measured in several recent works and controlled by the turbulence within the chamber[11,23,24,33] for 6−20 m^3 chambers. We do expect some dependence of the wall loss rate on chamber surface area to volume ratio[18] and show the results of a sensitivity study examining the wall loss rate later in the text. CF chambers have more turbulence due to the constant injection and removal of new air volumes. While many CF chambers do use fans for mixing, some CF chambers instead use pulses of injected air to mix the chamber contents more quickly, analogous to a fan.[34] We estimate a wall loss rate of 4 × 10^{-3} s^{-1} (mixing time scale of 250 s) for CF operation.[35] The faster timescale for wall loss of gases in CF

https://dx.doi.org/10.1021/acs.est.0c03381
Environ. Sci. Technol. 2020, 54, 12890−12897

chambers due to flow-induced mixing has not been recognized in past studies, to our knowledge.

We use kinetic and equilibrium partitioning theory to complete the modeling of the gas-phase losses. SVOC evaporates from the walls to reach equilibrium with its gas-phase concentration in the chamber,[21] and the evaporation rate can be calculated from the condensation rate and the equilibrium constant as:

$$k_{evap} = k_{cond}\frac{C^*}{C_w} \quad (1)$$

where C^* is the saturation vapor concentration and C_w is the equivalent wall mass concentration, by convention expressed as the equivalent amount of liquid organic aerosol particles that would result in the same gas-wall equilibrium condition.[21] In this work, we use the C^*-dependent parameterization of C_w determined in Krechmer et al.[23] for FEP Teflon walls (which likely implicitly accounts for higher activity coefficients in Teflon for more polar species[23]), resulting in a parameterization of $C_w = 16\ \mu g\ m^{-3}$ for $C^* < 1\ \mu g\ m^{-3}$.

The ELVOC, of much lower volatility, is assumed to partition irreversibly to the walls. Both the SVOC and ELVOC also condense on the preexisting inorganic seed into the aerosol phase with SVOC re-evaporating and ELVOC not. We keep track of the formed SOA from each of the condensing species, SVOA formed from the SVOC and LVOA formed from the LVOC. In the base model, we assume these species do not react further in the particle phase. We model partitioning from the particles consistent with recent detailed time-dependent studies.[11,33] The first-order condensation rate onto the particles is the suspended aerosol condensation sink (CS, s^{-1}). The model calculates a CS at each model time step based on the total amount of aerosol present at each point in the simulation (sum of seed aerosol, SVOA, and ELVOC OA) using the following equation

$$CS = \int_0^\infty r\ F_{FS}(r)N(r)\ dr \quad (2)$$

r is the particle radius, $N(r)$ is the particle number size distribution, and F_{FS} is the Fuchs−Sutugin correction for gas-phase diffusion,[36] where

$$F_{FS} = \frac{K_n + 1}{0.377\ K_n + 1 + \frac{4}{3}\alpha^{-1}K_n^{\ 2} + \frac{4}{3}\alpha^{-1}K_n} \quad (3)$$

Incorporating the CS, the model can then calculate a rate for gaseous condensation:

$$k = \frac{1}{4\pi \cdot D \cdot CS} \quad (4)$$

We use a diffusion coefficient of $D = 6 \times 10{-}6\ m^2\ s^{-1}$, assuming sea level pressure and 25 C.[37]

We assume a uniform distribution of 85 nm diameter particles;[13] a total aerosol density of 1.55 g cm^{-3},[38] and the abovementioned particle size. In the Fuchs−Sutugin correction, we use an accommodation coefficient (α) of 1.[11,33]

We treat SOA formation as a kinetic process that tends toward equilibrium, like gas-wall partitioning. The condensation sink is determined using the total amount of aerosol, including seed, but SOA partitioning is determined using a core-shell model. In this case, the seed aerosol is considered to form an inert core, and the amount of aerosol used to calculate partitioning fractions is the organic mass condensed around the ammonium sulfate seed core. The evaporation rate (k_{evap}) is calculated from the condensation rate (k_{cond}) and equilibrium constant as

$$k_{evap} = k_{cond}\frac{C^*}{c_{OA}} \quad (5)$$

where c_{OA} is the concentration of organic aerosol.[11,21] To spin up the model, we set the value of k_{evap} to 0 if c_{OA} is 0. This prevents the value of k_{evap} from becoming infinite and crashing the simulation during the first few time steps of the model before any organic aerosol forms.

SVOA molecules can evaporate from the particle or wall phases back into the gas phase. We assume the ELVOC molecules to be of very low volatility and remain in the condensed phases indefinitely. Both SVOA and ELVOA particles are lost to the chamber walls at a rate of 1×10^{-4} s^{-1}, typical of measured values in many chambers.[11,19,20] We treat particle-phase wall losses (also known as "particle wall loss") as irreversible and assume that the organic mass of particles deposited to the chamber walls mass does not participate in partitioning, as it has been shown that new Teflon chambers have indistinguishable losses from those in the old ones that were used in many high-concentration experiments.[21] Heterogeneous particle-phase chemistry is well documented in organic aerosol mass (e.g., ref 39), and we note that it is possible further chemical reactions occur in the organic mass of ELVOC and SVOC that deposit on the chamber walls. These particle-phase chemical transformations could alter the volatility of individual chemical species, resulting in their evaporation. We are, however, not aware of any direct experimental results demonstrating that the wall mass participates directly in partitioning.

To simplify the results of the base case and simulate an approximate correction for particle-phase wall losses, we set the particle-phase wall loss rate to 0. Figure S2 shows the model outputs with particle-phase losses included and in Figure S3 we show that because the yields determined with each method are the same, the results in this paper are not affected by this simplification.

To compare precursor fates between the CF and batch experiments, we also set up a batch version of the model. The batch version is identical to the CF version described above, but with the lower gas-phase wall loss rate (see above) and with no input flow or dilution of the bag contents. The model adds ozone at the same rate as in the CF model, and as in Shilling et al.[13] The theoretical ozone injection would add <0.1 L of volume to the 5 m^3 chamber, which we assume to have no effect on the experimental conditions. While batch experiments generally use faster oxidant injections, we hypothesize that faster injection would result in a higher condensation sink earlier in the experiment and decrease the effect of gas-phase wall losses relative to the CF experiment. Thus, we choose to inject ozone at the same rate in batch and CF modes. Both simulations run for 5 days, producing model outputs every 90 s (although the kinetic solver uses smaller time steps if needed).

To calculate an aerosol mass yield (Y), we mimic the methods of physical chamber experiment, either in batch or continuous flow mode. Y is calculated as follows

$$Y = \frac{M_{SOA}}{P_{Reacted}} \quad (6)$$

https://dx.doi.org/10.1021/acs.est.0c03381
Environ. Sci. Technol. 2020, 54, 12890−12897

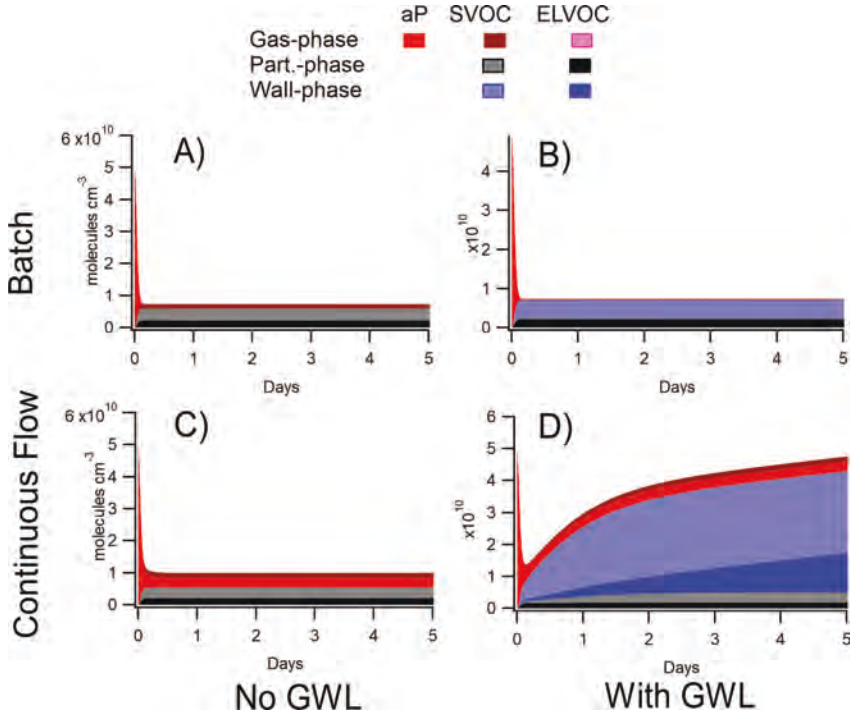

Figure 2. Concentrations of the organic compounds in the system as a function of simulation time. Other volatile gases present in the model are not included for clarity. To simplify the results of the base case and simulate an approximate correction for particle-phase wall losses, we set the particle-phase wall loss rate to 0 in all of the simulations shown here.

where M_{SOA} is the SOA mass concentration, and $P_{Reacted}$ is the amount of gas-phase precursor consumed by the reaction with ozone during the experiment.

In the batch mode simulation, we compute the maximum mass of SOA in the simulation, then divide it by the amount of α-pinene that reacted away during the simulation. In the CF chamber, we calculate the yield as the amount of SOA mass leaving the chamber divided by the amount of α-pinene precursor that is entering the reactor minus the unreacted fraction.

$$Y = \frac{M_{SOA}}{(P_{entering} - P_{unreacted})} \quad (7)$$

In the sensitivity studies, to evaluate the effect of GWL on the yield, we perturb the model by changing the kinetic input parameters (i.e., fractional product yields) for SVOC, ELVOC, and other gas formations, always keeping the total rate constant the same.

RESULTS AND DISCUSSION

Comparison of Batch and Continuous Flow Mode Simulations. Figure 2 shows stacked plots tracking the evolution of the precursor and products in gas, particle, and chamber walls phases.

The batch mode simulation reaches equilibrium after a few hours with and without GWL or with particle-phase wall losses enabled as shown in Figure S2, following the depletion of the α-pinene precursor and a few gas-wall timescales. Most of the mass ends up in the "other volatile gases" bulk species (Figure S4), as expected due to their much higher yield in the reaction with ozone. The ELVOC is completely in the condensed phases, as expected due to its low vapor pressure. When GWL are turned off, the SVOC surrogate compound is distributed with 69 and 31% in the particle and gas phases, respectively. When GWL is turned on, the SVOC compound ends up primarily in the walls. We note that there is an initially larger SVOC fraction on the particle phase, due to the shorter timescale for that equilibrium but then the walls "denude" the particles as expected (Figure S5).[24] As the Teflon walls of chambers represent a larger equivalent mass concentration (up to 10 mg m^{-3} depending on the volatility of the compound,[21] and 16 μg m^{-3} for the SVOC as simulated here), the SOA mass is too small to compete for the SVOC available to partition at equilibrium. This simulation shows that in so-called "atmospherically relevant" concentration batch experiments, in which low precursor and seed concentrations are used (comparable to those in forested areas where much of the α-pinene is oxidized globally), SVOC compounds will primarily partition to the walls of the chamber. In experiments at higher SOA concentrations, a larger SVOC fraction will be retained by the particles phase. E.g., we can estimate that for ~16 μg m^{-3} of SOA, SVOC will partition ~50/50 between the particle and the wall phases.

The loss of SVOC material to the walls remains significant in CF chambers (Figure 2D), substantially suppressing the aerosol yield over the first two experiment days. The net rate at which SVOC goes to the walls does approach zero after ~3 days of simulation time (Figure S5), signifying that the system is approaching gas-wall equilibrium. In other words, the continuous addition of SVOC mass to the walls has led to an accumulated amount that it is close to being able to sustain a gas-phase equilibrium concentration as if walls were not present. Thus, by generating enough SVOC and running the experiment under the same conditions for several days, it is possible for the SVOC to eventually come to equilibrium with the chamber walls (Figure S5). The need for several days per

https://dx.doi.org/10.1021/acs.est.0c03381
Environ. Sci. Technol. 2020, 54, 12890−12897

experiment does result in a reduced experiment throughput compared to typical batch chamber rates of an experiment per day. We also note that the detailed results for both types of chambers depend on the value of C_w (or equivalently, their activity coefficient in the Teflon film) for SVOC, which is uncertain.[11,23]

It is not possible, however, for the gas-phase ELVOC to come to equilibrium with the walls because its volatility is low enough to ensure its partitioning is irreversible to the first surface it encounters (Figure 2D), so any ELVOC lost to the walls are permanently lost from the SOA yield (Figure 3). Because the gas-phase wall loss rate in CF chambers will be higher than those run in batch mode (due to faster mixing), the wall loss rate is more competitive with the condensation sink in CF chambers. Thus, the proportion of gas ELVOC that end up in the walls is higher in CF mode than in batch mode (for the same CS).Plots of the condensation sink for the simulations shown in Figure 2 can be found in Figure S6.

Effect of Gas-Phase Wall Losses on Aerosol Mass Yields. Aerosol mass yield in the CF simulation increases the longer we wait to measure the yield (Figure 3A) due to the gradual suppression of SVOC losses as SVOC accumulates on the walls. Because the system takes 2−3 days to come to equilibrium and for yields to stabilize (Figure S4), yield measurements before that time are an underestimate. In this simulation, total losses of SVOC to the walls are effectively eliminated if the experiment lasts longer than 3 days with constant conditions. Generally, CF chamber experiments measure yields or chemical conditions after shorter periods of time, such as 12 to 24 h.[13,15] To compare batch and CF yields realistically, in Figure 3C we present the CF model SOA mass yields determined after 24 h of simulation time.

In the base CF simulation, at no measurement time does the yield with GWL reach the same level as the yield without GWL (Figure 3A). This is due to the irreversible and large ELVOC loss to the chamber walls. Without GWL, all perturbed simulations always provide the same yields, because without wall losses the condensation sink is the only fast sink for SVOC and ELVOC molecules. With GWL enabled, however, the yield becomes dependent on whether alternative sinks for the SVOC, and ELVOC outcompetes the gas-phase wall losses.

The sensitivity studies in the rest of Figure 3 examine simple mechanism variations as well as common experimental situations scientists use to mitigate the effects of wall losses on SOA yields in chamber studies. First, in Figure 3B we show yields from sensitivity studies perturbing the relative fraction of SVOC and ELVOC in the model. To evaluate with the model without semivolatile material, we turn off SVOC production, leaving only ELVOC produced. Without GWL, all the ELVOC partitions to the aerosol phase and remains there because there is no other competing source and no evaporation back into the particle phase. Despite the higher wall loss rate in the CF simulation, there is essentially no difference between the yields of the CF and batch ELVOC-only model runs. Also, of note is how the ELVOC-only CF simulation shows no yield time dependence, which only appears because of a semivolatile material coming to equilibrium.

For the SVOC-only case, we add a one-time starting concentration of ∼12 $\mu g\ m^{-3}$ (1 ppb) of ELVOC to the model as an organic aerosol seed, which is then diluted out over time and no longer present when yields are calculated. Otherwise, the SVOC-only case would form no aerosol with or without GWL. The ELVOC seed is not counted in calculating the

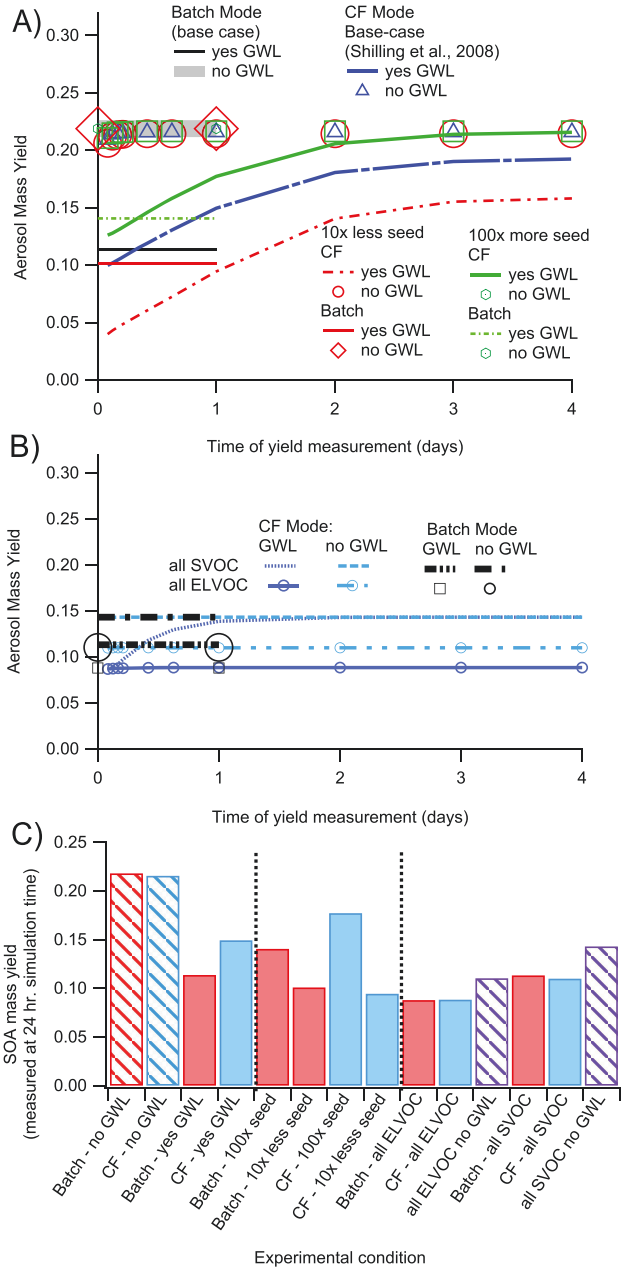

Figure 3. Aerosol mass yields as a function of simulation times for different model perturbations. (A) Shows aerosol mass yields from the base cases and determined from model runs perturbing the seed concentrations in the CF simulation. (B) Shows the yields determined from model runs perturbing the SVOC and ELVOC compound yields. (C) Shows yield values for the different sensitivity studies taken at 24 h of simulation time for batch and CF modes. Markers in (A) and (B) vary in size for visual clarity only.

SVOC-only yield. Both CF and batch mode simulations have almost identical yields under these conditions, and both show reduced yields compared to the simulation without GWL. We note that the SVOC-only case with GWL in Figure 3B does appear to reach yield equilibrium more quickly than many of the simulations in Figure 3A.

Next, we perturb the amount of starting seed aerosol in the chamber. We ran one set of simulations with 10× less seed (∼0.5 $\mu g\ m^{-3}$; CS = 0.002 s^{-1}) and one with 100× more seed

https://dx.doi.org/10.1021/acs.est.0c03381
Environ. Sci. Technol. 2020, 54, 12890−12897

than the starting amount (~500 μg m^{-3}; cs = 0.2 s^{-1}), both with and without GWL enabled. With GWL enabled, there are large differences in SOA yields throughout the experiment as the condensation sink and wall sink compete for available gas-phase molecules. Especially at early times (<2 days), higher amounts of seed can help partially overcome losses to the walls in both the CF and batch experiments. With 10× less seed, the yield is less than what is measured in the base case, as expected. In CF simulations, the yield gradually increases as gas-phase compounds accumulate and partition to the aerosol, forming a condensation sink large enough to compete with the walls. The yield with 10× less seed, however, never catches up to the base case simulation, demonstrating that the walls are more competitive with the smaller condensation sink for available vapors. On the other hand, using 100× more seed than the base case leads to a yield increase vs the base case. The higher seed allows the CF simulation to match the wall-less simulation yield at run times longer than 3 days. In the batch simulation, a higher starting seed results in a higher yield but not as high as the base case without GWL. In both simulations, a high starting seed makes the aerosol condensation sink faster the wall sink, allowing the particles to capture more ELVOC. But under typical experimental conditions (batch-mode base case and CF measured at <24 h), higher amounts of seed do not negate the effects of GWL on SOA yields.

Other works[15,19] have proposed that a lack of dependence of measured SOA yield on seed amount is evidence that CF chambers are not impacted by GWL. Liu et al.[15] showed a nominal ~10% increase in yield over a condensation sink increase by a factor of ~10. In Figure 4, we show model results over the same condensation sink range with varying wall loss rates. All other model parameters are kept the same as the base configuration described in Figure 1. To account for differences in yields between the α-pinene and isoprene systems, mass yields are plotted relative to the yield at the lowest surface area/CS by Liu et al.[15] The condensation sink values shown in Figure 4 were measured at the same time as the yield. The condensation sink calculation includes organic and seed aerosol together, to simulate an SMPS measurement.

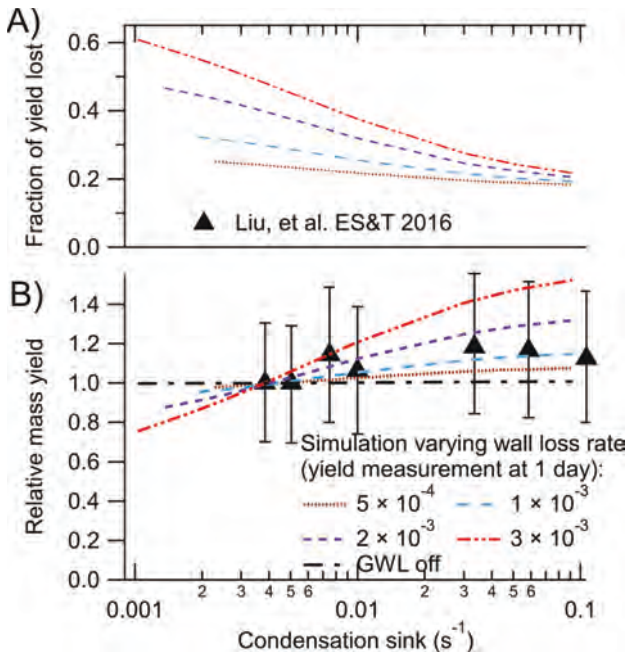

Figure 4. (A) Fraction of yield lost to GWL as a function of simulation condensation sink and wall loss rate k_{GWL}. (B) Comparison of relative yields for several model runs with the results from Liu et al.[15] Relative yields were determined relative to the average of the first two points shown in Liu et al. All simulations were run in CF mode for comparison against published CF studies. All model yields were corrected for PWL, though the ending CS values were determined without PWL corrections to best simulate the experimental data.

Figure 4B shows that this model reproduces the weak seed dependence previously reported by Liu et al.[15] and held as evidence by others[19] that GWL is not occurring in experiments. Despite the lack of aerosol CS dependence, gas-phase wall losses still occur in these simulations and strongly affect the SOA yields in each system. The relative yield-CS dependence varies by the gas-phase wall loss rate and inflects around the point where $k_{CS} \approx k_{GWL}$, i.e., when the loss rates of a gas-phase molecule to the walls and aerosol become equal. Thus, at CS values greater than the wall loss rate, a lack of seed dependence is not necessarily an indicator of whether gas-phase wall losses are taking place and certainly not of the magnitude. Indeed, in Figure 4A, we plot the fractional difference between the model yields shown in Figure 4B with GWL on and yields with GWL corrected. The results for a GWL rate of 1×10^{-3} s^{-1} are compatible with the experimental data within uncertainties, but still lose 25−35% of the yield to GWL depending on CS. But even high starting amounts of seed and chambers with low mixing rates lose 25% entirely due to gas-phase wall losses. These losses are almost entirely due to losses of SVOC, which can evaporate from particles and be scavenged by the faster wall loss sink. This SVOC loss results in the asymptote shown in Figure 4A, which occurs despite changes in the wall loss to the condensation sink ratio.

Despite previous claims to the contrary, gas-phase wall losses occur in CF and batch chambers and both require correction for accurate yield values even in experiments with high starting seed levels. Performing seed-dependent experiments over a larger range of CS, including cases where CS is lower than k_{GWL} is important to further characterize this issue. Examining the dependence of yield on time during the initial period of a CF experiment may also provide information to constrain GWL losses, as discussed above. While the phenomenology discussed here will apply to all chamber experiments, the quantitative details will vary with the chemical system under study and its chemical mechanisms, as well as the experimental and the chamber parameters.

Laboratory/Atmospheric Implications. Continuous flow chambers have been previously described as a superior method of determining SOA yields in laboratory experiments because they supposedly suffer from minimal effects of vapor wall loss. We show this belief to be incorrect with an experimentally constrained box model for typical operation parameters of CF chambers. Vapor wall loss effects on yields result from the near immediate competition of ELVOC condensation to walls (vs particles) and the long timescale for SVOC to reach equilibrium with chamber walls. It is still necessary for both CF and batch experiments to account for wall losses in yield determinations. While we understand that both modelers and experimentalists would like a formula or single equation that allows for an instant correction of yields for chamber wall loss (yield adjustment of X%), we note that gas-phase wall losses depend on many experimental parame-

https://dx.doi.org/10.1021/acs.est.0c03381
Environ. Sci. Technol. 2020, 54, 12890−12897

ters, as evidenced in this model. If it is not possible to reduce the effect of gas-phase wall losses by using higher concentrations, we recommend determining a correction by using a modeling framework as several groups have done with success.[40−42] Wall losses are largest in all types of chambers at low "atmospherically-relevant" conditions and are substantially reduced at higher concentrations.

■ ASSOCIATED CONTENT

Supporting Information

The Supporting Information is available free of charge at https://pubs.acs.org/doi/10.1021/acs.est.0c03381.

Results of model sensitivity studies exploring yield calculation methods, particle-phase wall loss corrections, and wall absorption (PDF)

■ AUTHOR INFORMATION

Corresponding Authors

Jordan E. Krechmer − *Aerodyne Research, Inc., Billerica, Massachusetts 01821, United States;* orcid.org/0000-0003-3642-0659; Phone: 978 633-9500; Email: krechmer@aerodyne.com

Jose L. Jimenez − *Cooperative Institute for Research in Environmental Sciences (CIRES) and Department of Chemistry, University of Colorado, Boulder, Colorado 80309, United States;* orcid.org/0000-0001-6203-1847; Phone: 303-492-3557; Email: jose.jimenez@colorado.edu; Fax: 303-492-1149

Author

Douglas A. Day − *Cooperative Institute for Research in Environmental Sciences (CIRES) and Department of Chemistry, University of Colorado, Boulder, Colorado 80309, United States;* orcid.org/0000-0003-3213-4233

Complete contact information is available at: https://pubs.acs.org/10.1021/acs.est.0c03381

Notes

The authors declare no competing financial interest.

■ ACKNOWLEDGMENTS

We acknowledge funding from DOE (BER/ASR) DE-SC0016559, DOE (SBIR) DE-SC0011218, NSF AGS-1740610 and AGS- 1822664, EPA STAR 83587701-0, and EPA STAR graduate fellowship (FP-91770901-0). This manuscript has not been reviewed by EPA, and thus no endorsement should be inferred.

■ REFERENCES

(1) Goldstein, A. H.; Galbally, I. E. Known and Unexplored Organic Constituents in the Earth's Atmosphere. *Environ. Sci. Technol.* **2007**, *41*, 1515−1521.

(2) Haagen-Smit, A. J. Chemistry and Physiology of Los Angeles Smog. *Ind. Eng. Chem.* **1952**, *44*, 1342−1346.

(3) Ng, N. L.; Kroll, J. H.; Chan, A. W. H.; Chhabra, P. S.; Flagan, R. C.; Seinfeld, J. H. Secondary Organic Aerosol Formation from *m*-Xylene, Toluene, and Benzene. *Atmos. Chem. Phys. Discuss.* **2007**, *7*, 4085−4126.

(4) Presto, A. A.; Huff Hartz, K. E.; Donahue, N. M. Secondary Organic Aerosol Production from Terpene Ozonolysis. 1. Effect of UV Radiation. *Environ. Sci. Technol.* **2005**, *39*, 7036−7045.

(5) Kim, P. S.; Jacob, D. J.; Fisher, J. A.; Travis, K. R.; Yu, K.; Zhu, L.; Yantosca, R. M.; Sulprizio, M. P.; Jimenez, J. L.; Campuzano-Jost, P.; Froyd, K. D.; Liao, J.; Hair, J. W.; Fenn, M. A.; Butler, C. F.; Wagner, N. L.; Gordon, T. D.; Welti, A.; Wennberg, P. O.; Crounse, J. D.; St. Clair, J. M.; Teng, A. P.; Millet, D. B.; Schwarz, J. P.; Markovic, M. Z.; Perring, A. E. Sources, Seasonality, and Trends of Southeast US Aerosol: An Integrated Analysis of Surface, Aircraft, and Satellite Observations with the GEOS-Chem Chemical Transport Model. *Atmos. Chem. Phys.* **2015**, *15* (18), 10411−10433.

(6) Hodzic, A.; Jimenez, J. L.; Madronich, S.; Canagaratna, M. R.; DeCarlo, P. F.; Kleinman, L.; Fast, J. Modeling Organic Aerosols in a Megacity: Potential Contribution of Semi-Volatile and Intermediate Volatility Primary Organic Compounds to Secondary Organic Aerosol Formation. *Atmos. Chem. Phys.* **2010**, *10*, 5491−5514.

(7) Cocker, D. R.; Flagan, R. C.; Seinfeld, J. H. State-of-the-Art Chamber Facility for Studying Atmospheric Aerosol Chemistry. *Environ. Sci. Technol.* **2001**, *35*, 2594−2601.

(8) Carter, W.; Cocker, D., III; Fitz, D.; Malkina, I.; Bumiller, K.; Sauer, C.; Pisano, J.; Bufalino, C.; Song, C. A New Environmental Chamber for Evaluation of Gas-Phase Chemical Mechanisms and Secondary Aerosol Formation. *Atmos. Environ.* **2005**, *39*, 7768−7788.

(9) Baltensperger, U.; Kalberer, M.; Dommen, J.; Paulsen, D.; Alfarra, M. R.; Coe, H.; Fisseha, R.; Gascho, A.; Gysel, M.; Nyeki, S.; Sax, M.; Steinbacher, M.; Prevot, A. S. H.; Sjögren, S.; Weingartner, E.; Zenobi, R. Secondary Organic Aerosols from Anthropogenic and Biogenic Precursors. *Faraday Discuss.* **2005**, *130*, 265−278. ; discussion 363-386, 519−524

(10) Pang, X.; Lewis, A. C.; Rickard, A. R.; Baeza-Romero, M. T.; Adams, T. J.; Ball, S. M.; Daniels, M. J. S.; Goodall, I. C. A.; Monks, P. S.; Peppe, S.; Ródenas García, M.; Sánchez, P.; Muñoz, A. A Smog Chamber Comparison of a Microfluidic Derivatisation Measurement of Gas-Phase Glyoxal and Methylglyoxal with Other Analytical Techniques. *Atmos. Meas. Tech.* **2014**, *7*, 373−389.

(11) Krechmer, J. E.; Day, D. A.; Ziemann, P. J.; Jimenez, J. L. Direct Measurements of Gas/Particle Partitioning and Mass Accommodation Coefficients in Environmental Chambers. *Environ. Sci. Technol.* **2017**, *51*, 11867−11875.

(12) Poppe, D.; Brauers, T.; Dorn, H.-P.; Karl, M.; Mentel, T.; Schlosser, E.; Tillmann, R.; Wegener, R.; Wahner, A. OH-Initiated Degradation of Several Hydrocarbons in the Atmosphere Simulation Chamber SAPHIR. *J. Atmos. Chem.* **2007**, *57*, 203−214.

(13) Shilling, J. E.; Chen, Q.; King, S. M.; Rosenoern, T.; Kroll, J. H.; Worsnop, D. R.; McKinney, K. A.; Martin, S. T. Particle Mass Yield in Secondary Organic Aerosol Formed by the Dark Ozonolysis of α-Pinene. *Atmos. Chem. Phys.* **2008**, *8*, 2073−2088.

(14) Kirkby, J.; Curtius, J.; Almeida, J.; Dunne, E.; Duplissy, J.; Ehrhart, S.; Franchin, A.; Gagné, S.; Ickes, L.; Kürten, A.; Kupc, A.; Metzger, A.; Riccobono, F.; Rondo, L.; Schobesberger, S.; Tsagkogeorgas, G.; Wimmer, D.; Amorim, A.; Bianchi, F.; Breitenlechner, M.; David, A.; Dommen, J.; Downard, A.; Ehn, M.; Flagan, R. C.; Haider, S.; Hansel, A.; Hauser, D.; Jud, W.; Junninen, H.; Kreissl, F.; Kvashin, A.; Laaksonen, A.; Lehtipalo, K.; Lima, J.; Lovejoy, E. R.; Makhmutov, V.; Mathot, S.; Mikkilä, J.; Minginette, P.; Mogo, S.; Nieminen, T.; Onnela, A.; Pereira, P.; Petäjä, T.; Schnitzhofer, R.; Seinfeld, J. H.; Sipilä, M.; Stozhkov, Y.; Stratmann, F.; Tomé, A.; Vanhanen, J.; Viisanen, Y.; Vrtala, A.; Wagner, P. E.; Walther, H.; Weingartner, E.; Wex, H.; Winkler, P. M.; Carslaw, K. S.; Worsnop, D. R.; Baltensperger, U.; Kulmala, M. Role of Sulphuric Acid, Ammonia and Galactic Cosmic Rays in Atmospheric Aerosol Nucleation. *Nature* **2011**, *476*, 429−433.

(15) Liu, J.; D'Ambro, E. L.; Lee, B. H.; Lopez-Hilfiker, F. D.; Zaveri, R. A.; Rivera-Rios, J. C.; Keutsch, F. N.; Iyer, S.; Kurten, T.; Zhang, Z.; Gold, A.; Surratt, J. D.; Shilling, J. E.; Thornton, J. A. Efficient Isoprene Secondary Organic Aerosol Formation from a Non-IEPOX Pathway. *Environ. Sci. Technol.* **2016**, *50*, 9872−9880.

(16) Riva, M.; Rantala, P.; Krechmer, J. E.; Peräkylä, O.; Zhang, Y.; Heikkinen, L.; Garmash, O.; Yan, C.; Kulmala, M.; Worsnop, D.; Ehn, M. Evaluating the Performance of Five Different Chemical Ionization Techniques for Detecting Gaseous Oxygenated Organic Species. *Atmos. Meas. Tech.* **2019**, *12*, 2403−2421.

(17) Zaytsev, A.; Koss, A. R.; Breitenlechner, M.; Krechmer, J. E.; Nihill, K. J.; Lim, C. Y.; Rowe, J. C.; Cox, J. L.; Moss, J.; Roscioli, J. R.; Canagaratna, M. R.; Worsnop, D. R.; Kroll, J. H.; Keutsch, F. N. Mechanistic Study of the Formation of Ring-Retaining and Ring-Opening Products from the Oxidation of Aromatic Compounds under Urban Atmospheric Conditions. *Atmos. Chem. Phys.* **2019**, *19*, 15117−15129.

(18) McMurry, P. H.; Grosjean, D. Gas and Aerosol Wall Losses in Teflon Film Smog Chambers. *Environ. Sci. Technol.* **1985**, *19*, 1176−1182.

(19) Nah, T.; McVay, R. C.; Pierce, J. R.; Seinfeld, J. H.; Ng, N. L. Constraining Uncertainties in Particle-Wall Deposition Correction during SOA Formation in Chamber Experiments. *Atmos. Chem. Phys.* **2017**, *17*, 2297−2310.

(20) Wang, N.; Jorga, S. D.; Pierce, J. R.; Donahue, N. M.; Pandis, S. N. Particle Wall-Loss Correction Methods in Smog Chamber Experiments. *Atmos. Meas. Tech.* **2018**, *11*, 6577−6588.

(21) Matsunaga, A.; Ziemann, P. J. Gas-Wall Partitioning of Organic Compounds in a Teflon Film Chamber and Potential Effects on Reaction Product and Aerosol Yield Measurements. *Aerosol Sci. Technol.* **2010**, *44*, 881−892.

(22) Zhang, X.; Cappa, C. D.; Jathar, S. H.; McVay, R. C.; Ensberg, J. J.; Kleeman, M. J.; Seinfeld, J. H. Influence of Vapor Wall Loss in Laboratory Chambers on Yields of Secondary Organic Aerosol. *Proc. Natl. Acad. Sci. U. S. A.* **2014**, *111*, 5802−5807.

(23) Krechmer, J. E.; Pagonis, D.; Ziemann, P. J.; Jimenez, J. L. Quantification of Gas-Wall Partitioning in Teflon Environmental Chambers Using Rapid Bursts of Low-Volatility Oxidized Species Generated in Situ. *Environ. Sci. Technol.* **2016**, *50*, 5757−5765.

(24) Ye, P.; Ding, X.; Hakala, J.; Hofbauer, V.; Robinson, E. S.; Donahue, N. M. Vapor Wall Loss of Semi-Volatile Organic Compounds in a Teflon Chamber. *Aerosol Sci. Technol.* **2016**, *50*, 822−834.

(25) Huang, Y.; Zhao, R.; Charan, S. M.; Kenseth, C. M.; Zhang, X.; Seinfeld, J. H. Unified Theory of Vapor−Wall Mass Transport in Teflon-Walled Environmental Chambers. *Environ. Sci. Technol.* **2018**, *52*, 2134−2142.

(26) Kokkola, H.; Yli-Pirilä, P.; Vesterinen, M.; Korhonen, H.; Keskinen, H.; Romakkaniemi, S.; Hao, L.; Kortelainen, A.; Joutsensaari, J.; Worsnop, D. R.; Virtanen, A.; Lehtinen, K. E. J. The Role of Low Volatile Organics on Secondary Organic Aerosol Formation. *Atmos. Chem. Phys.* **2014**, *14*, 1689−1700.

(27) Pankow, J. F. An Absorption Model of Gas/Particle Partitioning of Organic Compounds in the Atmosphere. *Atmos. Environ.* **1994**, *28*, 185−188.

(28) Peng, Z.; Jimenez, J. L. KinSim: A Research-Grade, User-Friendly, Visual Kinetics Simulator for Chemical-Kinetics and Environmental-Chemistry Teaching. *J. Chem. Educ.* **2019**, *96*, 806−811.

(29) Calvert, J. G.; Atkinson, R.; Kerr, J. A.; Madronich, S.; Moortgat, G. K.; Wallington, T. J.; Yarwood, G. *The Mechanisms of Atmospheric Oxidation Ofthe Alkenes*; Oxford University Press: New York, 2000.

(30) Isaacman-VanWertz, G.; Massoli, P.; O'Brien, R.; Lim, C.; Franklin, J. P.; Moss, J. A.; Hunter, J. F.; Nowak, J. B.; Canagaratna, M. R.; Misztal, P. K.; Arata, C.; Roscioli, J. R.; Herndon, S. T.; Onasch, T. B.; Lambe, A. T.; Jayne, J.; Su, L.; Knopf, D. A.; Goldstein, A. H.; Worsnop, D. R.; Kroll, J. H. Chemical Evolution of Atmospheric Organic Carbon over Multiple Generations of Oxidation. *Nat. Chem.* **2017**, *10*, 462.

(31) Ehn, M.; Thornton, J. A.; Kleist, E.; Sipilä, M.; Junninen, H.; Pullinen, I.; Springer, M.; Rubach, F.; Tillmann, R.; Lee, B.; Lopez-Hilfiker, F.; Andres, S.; Acir, I.-H.; Rissanen, M.; Jokinen, T.; Schobesberger, S.; Kangasluoma, J.; Kontkanen, J.; Nieminen, T.; Kurtén, T.; Nielsen, L. B.; Jørgensen, S.; Kjaergaard, H. G.; Canagaratna, M.; Maso, M. D.; Berndt, T.; Petäjä, T.; Wahner, A.; Kerminen, V.-M.; Kulmala, M.; Worsnop, D. R.; Wildt, J.; Mentel, T. F. A Large Source of Low-Volatility Secondary Organic Aerosol. *Nature* **2014**, *506*, 476−479.

(32) Tröstl, J.; Chuang, W. K.; Gordon, H.; Heinritzi, M.; Yan, C.; Molteni, U.; Ahlm, L.; Frege, C.; Bianchi, F.; Wagner, R.; Simon, M.; Lehtipalo, K.; Williamson, C.; Craven, J. S.; Duplissy, J.; Adamov, A.; Almeida, J.; Bernhammer, A.-K.; Breitenlechner, M.; Brilke, S.; Dias, A.; Ehrhart, S.; Flagan, R. C.; Franchin, A.; Fuchs, C.; Guida, R.; Gysel, M.; Hansel, A.; Hoyle, C. R.; Jokinen, T.; Junninen, H.; Kangasluoma, J.; Keskinen, H.; Kim, J.; Krapf, M.; Kürten, A.; Laaksonen, A.; Lawler, M.; Leiminger, M.; Mathot, S.; Möhler, O.; Nieminen, T.; Onnela, A.; Petäjä, T.; Piel, F. M.; Miettinen, P.; Rissanen, M. P.; Rondo, L.; Sarnela, N.; Schobesberger, S.; Sengupta, K.; Sipilä, M.; Smith, J. N.; Steiner, G.; Tomè, A.; Virtanen, A.; Wagner, A. C.; Weingartner, E.; Wimmer, D.; Winkler, P. M.; Ye, P.; Carslaw, K. S.; Curtius, J.; Dommen, J.; Kirkby, J.; Kulmala, M.; Riipinen, I.; Worsnop, D. R.; Donahue, N. M.; Baltensperger, U. The Role of Low-Volatility Organic Compounds in Initial Particle Growth in the Atmosphere. *Nature* **2016**, *533*, 527−531.

(33) Liu, X.; Day, D. A.; Krechmer, J. E.; Brown, W.; Peng, Z.; Ziemann, P. J.; Jimenez, J. L. Direct Measurements of Semi-Volatile Organic Compound Dynamics Show near-Unity Mass Accommodation Coefficients for Diverse Aerosols. *Commun. Chem.* **2019**, *2*, 98.

(34) Nguyen, T. B.; Crounse, J. D.; Schwantes, R. H.; Teng, A. P.; Bates, K. H.; Zhang, X.; St. Clair, J. M.; Brune, W. H.; Tyndall, G. S.; Keutsch, F. N.; Seinfeld, J. H.; Wennberg, P. O. Overview of the Focused Isoprene EXperiment at the California Institute of Technology (FIXCIT): Mechanistic Chamber Studies on the Oxidation of Biogenic Compounds. *Atmos. Chem. Phys.* **2014**, *14*, 13531−13549.

(35) Finewax, Z.; Jimenez, J. L.; Ziemann, P. J. Development and Application of a Low-Cost Vaporizer for Rapid, Quantitative Addition of Organic Gases and Particles to an Environmental Chamber. *Aerosol Sci. Technol.* **2020**, *27* (2), 1−12.

(36) Seinfeld, J. H.; Pandis, S. N. *Atmospheric Chemistry and Physics: From Air Pollution to Climate Change*; 2nd ed.; John Wiley & Sons, Inc.: Hoboken, New Jersey, USA, 2006; Vol. *2nd*.

(37) Tang, M. J.; Shiraiwa, M.; Pöschl, U.; Cox, R. A.; Kalberer, M. Compilation and Evaluation of Gas Phase Diffusion Coefficients of Reactive Trace Gases in the Atmosphere: Volume 2. Diffusivities of Organic Compounds, Pressure-Normalised Mean Free Paths, and Average Knudsen Numbers for Gas Uptake Calculations. *Atmos. Chem. Phys.* **2015**, *15*, 5585−5598.

(38) Shilling, J. E.; Chen, Q.; King, S. M.; Rosenoern, T.; Kroll, J. H.; Worsnop, D. R.; Decarlo, P. F.; Aiken, A. C.; Sueper, D.; Jimenez, J. L.; Martin, S. T. Loading-Dependent Elemental Composition of α-Pinene SOA Particles. *Atmos. Chem. Phys.* **2009**, *9*, 771−782.

(39) Shiraiwa, M.; Yee, L. D.; Schilling, K. A.; Loza, C. L.; Craven, J. S.; Zuend, A.; Ziemann, P. J.; Seinfeld, J. H. Size Distribution Dynamics Reveal Particle-Phase Chemistry in Organic Aerosol Formation. *Proc. Natl. Acad. Sci. U. S. A.* **2013**, *110*, 11746−11750.

(40) Pratap, V.; Bian, Q.; Kiran, S. A.; Hopke, P. K.; Pierce, J. R.; Nakao, S. Investigation of Levoglucosan Decay in Wood Smoke Smog-Chamber Experiments: The Importance of Aerosol Loading, Temperature, and Vapor Wall Losses in Interpreting Results. *Atmos. Environ.* **2018**, *199*, 224−232.

(41) Bian, Q.; May, A. A.; Kreidenweis, S. M.; Pierce, J. R. Investigation of Particle and Vapor Wall-Loss Effects on Controlled Wood-Smoke Smog-Chamber Experiments. *Atmos. Chem. Phys.* **2015**, *15*, 11027−11045.

(42) He, Y.; King, B.; Pothier, M.; Lewane, L.; Akherati, A.; Mattila, J.; Farmer, D. K.; McCormick, R. L.; Thornton, M.; Pierce, J. R.; Volckens, J.; Jathar, S. H. Secondary Organic Aerosol Formation from Evaporated Biofuels: Comparison to Gasoline and Correction for Vapor Wall Losses. *Environ. Sci. Process. Impacts* **2020**, 1461.

https://dx.doi.org/10.1021/acs.est.0c03381
Environ. Sci. Technol. 2020, 54, 12890−12897